Ultrafast all-optical logic gates, optical limiting and all-optical diode with *Hibiscus sabdariffa* dye

ANAM SAIFI, SUKHDEV ROY*
Department of Physics and Computer Science, Dayalbagh Educational Institute, Dayalbagh, Agra-282005, India

Femtosecond saturable and reverse saturable absorption in *Hibiscus sabdariffa* dye has been theoretically studied with 40 fs laser pulses at 515 nm and 1030 nm, respectively. Theoretical simulations agree well with reported experimental results. Ultrafast all-optical OR and AND logic gates at 515 nm, as well as NOT, universal NOR and NAND logic gates at 1030 nm have been designed based on optimization of nonlinear absorption to achieve enhanced contrast and low-power operation. An optical limiter and all-optical diode have also been designed demonstrating the material's ultrafast performance, tunability, stability, and versatility for practical applications.

(Received February 26, 2025 accepted April 6, 2026)

Keywords: Hibiscus sabdariffa dye, Ultrafast nonlinear absorption, All-optical logic gates, All-optical diode, Optical limiting

1. Introduction

The pursuit of ultrafast all-optical (AO) information processing has garnered significant attention, aiming to harness light-matter interactions to surpass the performance of traditional electronic circuits. To realize this vision, the development of efficient AO switches with rapid response times, high contrast, and minimal power consumption is essential [1,2]. Additionally, other desired features include ease of fabrication, small footprint, cost-effectiveness, reconfigurability, tunability of its properties, durability, low insertion losses, high extinction ratio, photothermal and chemical stability as well as the scalability to integrate into circuits and networks [3,4].

A diverse variety of organic and inorganic nonlinear optical (NLO) materials has been explored for photonic applications. These materials include azobenzene, porphyrins, phthalocyanines, rhodopsins, fluorophores, chromophores, green fluorescence protein, photoactive yellow protein, semiconductor doped glasses, fullerenes, push-pull organic conjugated system, covalent and metal-organic framework films, graphene and its nanofilms, transition metal oxides and transition metal dichalcogenides, DNA biopolymer doped with natural dyes, two-dimensional materials, twistacenes, MXenes, perovskites, quasi 2D perovskites and nonlinear plasmonic metasurfaces [5–34].

Among organic NLO materials, naturally occurring plant and fruit-derived natural pigment and dyes also exhibit strong NLO properties, and cost effectiveness making them attractive alternatives to synthetic dyes in photonic technologies [35–44]. NLO characterization that includes nonlinear absorption (NLA), nonlinear refraction (NLR) and two-photon absorption (TPA) in beetroot, blackberry, cherry, red cabbage, curcumin derivatives, tea, henna, β-carotenoids, pumpkin seed oil, turmeric, betanins, chlorophylls, and natural tomato has been reported and some AO device applications such as signal modulation, switching, and optical limiting have also been demonstrated with cw and pulsed lasers [36-44]. These materials exhibit broad absorption profiles and rapid response times [47].

Natural dyes from the anthocyanin family exhibit notable optical properties, including significant NLA and NLR [37,38,48]. Variations in the composition of anthocyanin-based organic dyes lead to noticeable changes in the intensity and position of the absorption bands, which in turn affect both the NLA coefficients and nonlinear refractive index, largely due to their molecular structure [49].

The *Hibiscus sabdariffa* flower is abundant in anthocyanins, making its extract a promising candidate for exploring NLO properties. Its NLO characteristics arise from the significant number of delocalized π-electrons within the anthocyanin structure, which contribute to strong 3rd harmonic generation, TPA, and intensity-dependent refractive index [50,51]. The different NLO properties of *H. sabdariffa* have been experimentally explored with continuous wave and pulsed lasers [45,48,50–53]. Various materials have been integrated with *H. sabdariffa* dye to improve its performance for specific applications in the biosynthesis of nanoparticles, antibacterial, anticancer and photocatalytic activities, bioimaging, sensing, broadband photodetector, dye sensitized solar cells and textile industries [54–56].

Recently, ultrafast NLO and transient absorption (TA) studies on *Hibiscus sabdariffa* dye have been reported with laser pulses of pulse duration 40 fs at wavelengths of 515 nm and 1030 nm [50]. The dye demonstrates a notable negative NLA coefficient (β) of -2.7×10^{-11} cm/W at 515 nm, whereas it shows a positive NLA coefficient of $+2.1 \times 10^{-13}$ cm/W at 1030 nm. The TA decay experiments with fs laser pulses of pulse duration 40 fs at 515 nm indicate a rapid relaxation time of approximately 3 ps, which is associated with the excited state proton transfer process [50,51].

AO logic gates and AO diodes (AODs) are crucial components in AO computing and networks. An AOD can be formed based on axially asymmetric NLA, which is achieved by placing a saturable absorber material adjacent to a reverse saturable absorber material. *Hibiscus sabdariffa* exhibits both saturable absorption (SA) and reverse saturable absorption (RSA) properties at 515 nm and 1030 nm, respectively. Thus, by simply adjusting the wavelength, an AOD can be realized with *H. sabdariffa* extract. Its ultrafast NLA response outperforms many other naturally occurring organic dyes, making it an interesting candidate for AO device applications [36,38].

Hence, the objective of this paper is to: (i) conduct a comprehensive theoretical study of fs NLA dynamics in *Hibiscus sabdariffa* dye, (ii) study the effect of input intensity (I_o), effective path length (L) and NLA coefficient (β) on SA and RSA characteristics, and determine the optimal photostimulated conditions for the design of (iii) ultrafast AO OR, AND, NOT, as well as the universal logic gates, NAND and NOR, (iv) optical limiter and (v) AO diode.

2. Theoretical model

Ultrafast NLA of *Hibiscus sabdariffa* dye in the fs regime can be interpreted using a two-level energy model as represented in Fig. 1 [50,57–59]. The ground-state (S_0) exhibits low absorption at the excitation wavelength of 1030 nm, where the energy of photon is nearly half the energy difference between the S_0 and the excited state (S_1). Electrons make a TPA-induced transition from S_0 to S_1, as they cannot make direct transition to S_1 due to less photon energy than the excitation energy. Hence, TPA is the dominant NLA mechanism under the laser input intensity of pulse duration 40 fs laser at 1030 nm. The fs TA experiments with *H. sabdariffa* dye reveal that the excited-state population has a lifetime of about 3 ps, which is too short for the population buildup necessary for excited state absorption [50]. At λ = 515 nm, the electrons from S_0 make transition to S_1 with one-photon absorption (OPA) that results in SA.

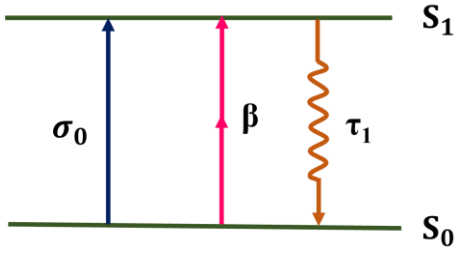

Fig. 1. Energy-level diagram for Hibiscus sabdariffa dye (colour online)

The temporal variation of population densities in various energy states at 1030 nm are expressed as,

$$\frac{dn_{S_0}}{dt} = -\frac{\sigma_0 I_{in} n_{S_0}}{h\upsilon} - \frac{\beta I_{in}^2}{2h\upsilon} + \frac{n_{S_1}}{\tau_1} \tag{1}$$

$$\frac{dn_{S_1}}{dt} = \frac{\sigma_0 I_{in} n_{S_0}}{h\upsilon} - \frac{n_{S_1}}{\tau_1} + \frac{\beta I_{in}^2}{2h\upsilon} \quad \text{with } n_{S_0} + n_{S_1} = n \tag{2}$$

where n_{S_0} and n_{S_1} are the population distribution of the S_0 and S_1 states, respectively. σ_0 denotes the absorption cross-section of S_0, τ_1 is the lifetime of S_1 and β is TPA coefficient as shown in Fig. 1.

The intensity (I) of the transmitted light through the sample is expressed as,

$$\frac{dI}{dz} = -\sigma_0 n_{S_0} I_{in} - \beta I_{in}^2 \tag{3}$$

The input Gaussian pulse is expressed as,

$$I_{in} = I_o \left(\frac{\omega_0^2}{\omega^2(z)}\right) exp\left(-\frac{t^2}{\tau_P^2}\right) exp\left(-\frac{2r^2}{\omega^2(z)}\right) \tag{4}$$

where $\omega(z) = \omega_0\left(1 + \left(\frac{z}{z_0}\right)^2\right)^{1/2}$, $z_0 = \frac{\pi\omega_0^2}{\lambda}$, ω_0 is the beam waist radius, z_0 is the Rayleigh range, τ_P is the pulse-width, and I_o is the peak input intensity. Given that, $z << z_0$ and $\omega(z) = \omega_0$, the sample is considered to be positioned at the beam's focal point, neglecting propagation effects. Rayleigh length is considered to be sufficiently larger than the sample path length to avoid the propagation effects.

Ultrafast AO logic gates may be realized by considering binary inputs Gaussian laser pulses with maximum pulse peaks occur at t_{m1}, t_{m2} and t_{m3} as follows [10]:

$$I_{input\ 1} = I_o \frac{\omega_0^2}{\omega^2(z)}\left[exp\left(-c\left(\frac{t - t_{m1}}{\tau_P}\right)^2\right) + exp\left(-c\left(\frac{t - t_{m2}}{\tau_P}\right)^2\right)\right] exp\left(-\frac{2r^2}{\omega^2(z)}\right) \tag{5}$$

and

$$I_{input\ 2} = I_o \frac{\omega_0^2}{\omega^2(z)}\left[exp\left(-c\left(\frac{t - t_{m3}}{\tau_P}\right)^2\right) + exp\left(-c\left(\frac{t - t_{m2}}{\tau_P}\right)^2\right)\right] exp\left(-\frac{2r^2}{\omega^2(z)}\right) \tag{6}$$

The nonreciprocity of an AOD can be determined by the following equation [60]:

$$dB = 10 \times log\left(\frac{T_{forward}}{T_{reverse}}\right) \tag{7}$$

where the nonlinear transmittance values for forward and reverse directions are represented by $T_{forward}$ and $T_{reverse}$, respectively.

3. Results and discussion

Numerical simulations have been used to analyse ultrafast NLA in *Hibiscus sabdariffa* dye by considering equations (1-4). The study is based on reported experiments with fs laser pulses at a 1 kHz repetition rate, functioning at 515 nm and 1030 nm to excite the sample, with experimental parameters, $\sigma_0 = 1.2 \times 10^{-21}$ cm^2, $\omega_0 = 55$ µm, $\tau_P = 40$ fs, $\tau_1 = 2.8$ ps, concentration = 81 mM, $\beta = -1 \times 10^{-11}$ cm/W at 515 nm, $\beta = 1.7 \times 10^{-13}$ cm/W and 1.3×10^{-12} cm/W at 1030 nm for L = 1 mm and 2 mm, respectively [50].

The Fig. 2 illustrates the time-dependent transmittance with *Hibiscus sabdariffa* dye in distilled water for various I_o values. As illustrated in Figs. 2(a) and 2(b), SA is evident at 515 nm, while RSA is observed at 1030 nm. The maximum percentage modulation achieved for RSA is 70% at $I_o = 5 \times 10^{12}$ W/cm^2 (Fig. 2 (b)). The time-dependent change in normalized population density is presented in Fig. 3, which shows that the population of S_0 decreases with a corresponding build-up of the population of S_1 (Fig. 3(a) and 3(b)). The results from the theoretical simulations align closely with the experimentally reported ultrafast Z-scan open aperture results [50].

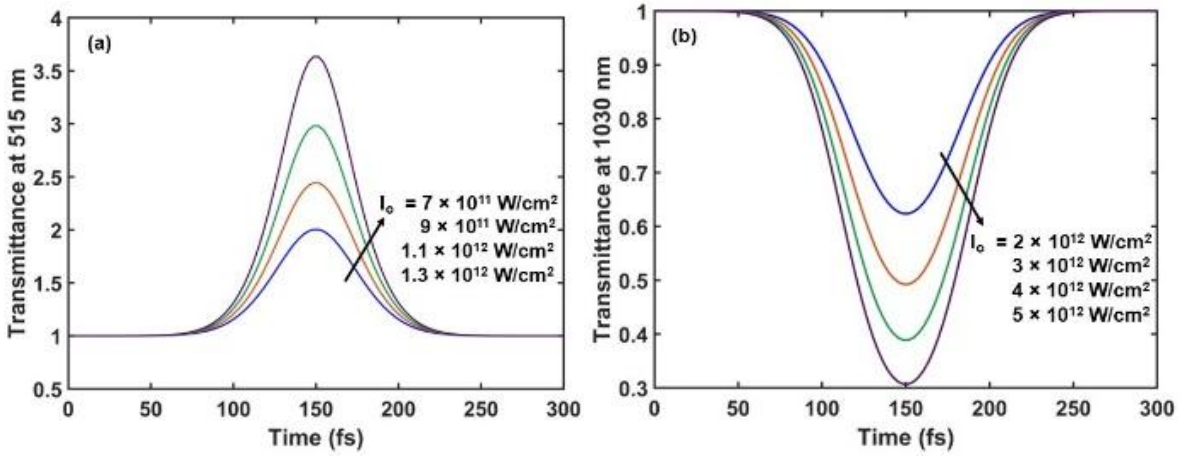

Fig. 2. Time-dependent change in transmittance during 40 fs pulse under varying I_o values at: (a) L= 1 mm and $\beta = -1 \times 10^{-11}$ cm/W, (b) L = 2 mm and $\beta = 1.3 \times 10^{-12}$ cm/W (colour online)

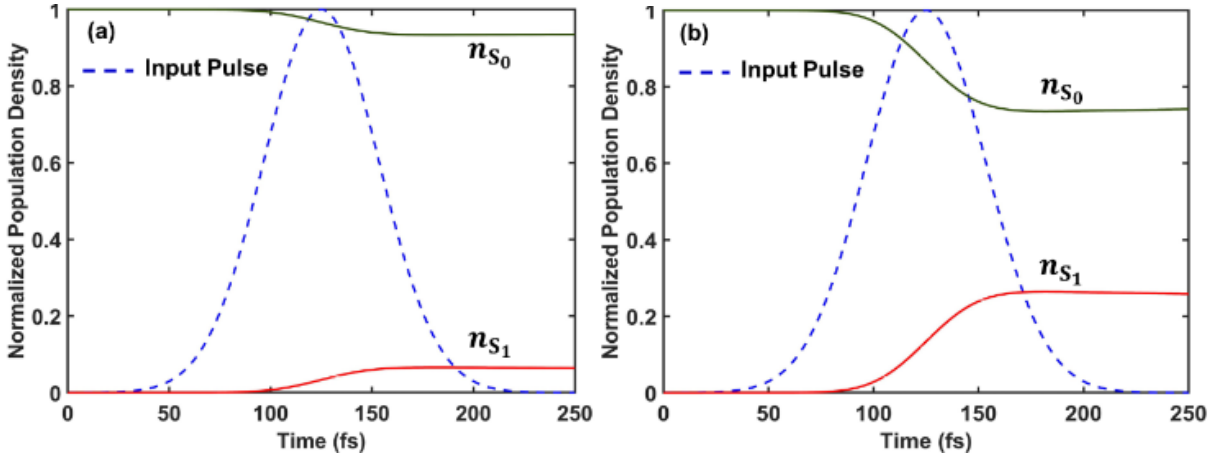

Fig. 3. Time-dependent change in normalized population densities at 1030 nm and $\tau_P = 40$ fs for different I_o values: (a) 2×10^{12} W/cm^2, (b) 4×10^{12} W/cm^2 (colour online)

The variation in RSA with change in L values is shown in Fig. 4 (a). On increasing L, the transmittance gradually decreases and then saturates. The maximum percentage modulation is 86% at $I_o = 4.9 \times 10^{12}$ W/cm^2 and L = 6 mm. This is due to the increased absorbance, which enhances the probability of photon-molecule interactions for a larger sample size [50]. It has been shown that NLA's dependence on the L suggests that NLA surpasses NLR. As a result, it can be deduced that the self-focusing effect seen in the *Hibiscus sabdariffa* dye under intense pulses is a result of the nonlinear Kerr effect, induced by the excitation of chromophores by the incoming pulses [50, 51]. But increasing the sample size will lead to the bulky optical circuits and impractical for future technological advancements.

The RSA properties also depend on the value of the TPA coefficient, as illustrated in Fig. 4(b). As the β values increase, the percentage modulation also increases. At β = 4

$\times 10^{-12}$ cm/W, maximum percentage modulation is 97.16% at $I_o = 4.9 \times 10^{12}$ W/cm^2, and L = 2 mm.

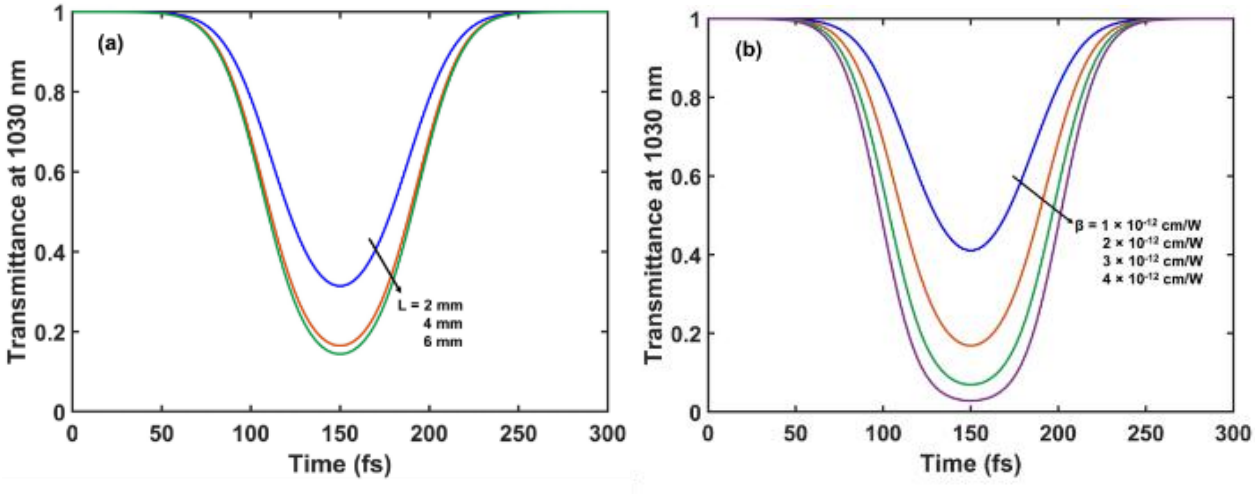

Fig. 4. Time-dependent change in transmittance during 40 fs pulse for different values of: (a) L at $I_o = 4.9 \times 10^{12}$ W/cm^2, (b) β at $I_o = 4.9 \times 10^{12}$ W/cm^2 and L = 2 mm (colour online)

The RSA characteristics have been used to study optical limiting at 1030 nm as shown in Fig. 5 that exhibits the suitability of *Hibiscus sabdariffa* dye for this important application [61]. The optical limiting threshold, defined at 90% of the linear transmittance, was found to be at 7×10^{11} W/cm^2. A stronger attenuation point corresponding to 50% transmission reduction occurs at 4×10^{12} W/cm^2, indicating the deep nonlinear absorption regime. The clamping threshold transmittance, which is the maximum output level beyond which the transmitted intensity does not increase significantly, even if input keeps increasing is 0.43.

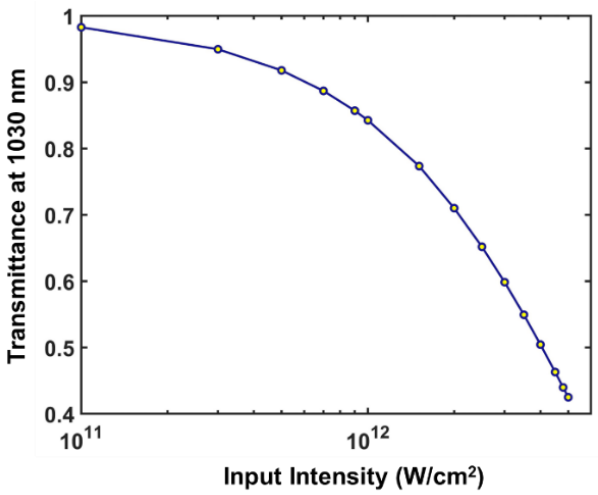

Fig. 5. Femtosecond optical limiter with Hibiscus sabdariffa dye at 1030 nm, $\omega_0 = 25$ μm and $\tau_P = 40$ fs (colour online)

The wavelength-dependent SA and RSA characteristics of dye have been utilized to theoretically design ultrafast AO binary logic gates, including OR, AND, NOT as well as the universal gates. To achieve this, theoretical simulations were performed by considering two input Gaussian laser pulses as expressed in equations (5) and (6) of equal intensity at 515 nm for OR, AND and at 1030 nm for NOT and the universal Boolean logic gates, to excite the sample. The maximum input pulse intensities considered for SA and RSA are below 1.4 TW/cm^2 and 5 TW/cm^2, respectively, at which reported z-scan experiments have been performed and no thermal effects have been observed [50].

The SA characteristics are utilized to design ultrafast AO OR and AND Boolean logic gates using two input pulses of equal intensity, each with $I_o = 6.5 \times 10^{11}$ W/cm^2 as shown in Fig. 6. The transmittance through the sample for each individual pulse is 1.89. However, when both the pulses are incident together, the combined input intensity leads to an increase in transmittance because of the SA. Without setting a threshold value of transmittance, this configuration enables ultrafast AO OR Boolean logic gate functionality. The output will be high when at least one of the pulses is present, and low when neither pulse is present, as shown in Fig. 6. By setting a transmittance threshold value at 1.89 (dashed line), the identical set up functions as an ultrafast AO AND logic, producing the high output only when both pulses are incident at the same time.

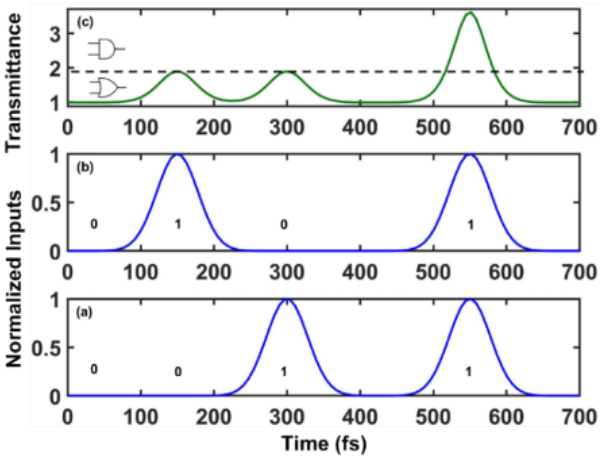

Fig. 6. Time-dependent change in output transmittance at 515 nm and design of ultrafast AO binary inputs logic gates (with a threshold of 1.89, shown by the dashed line): (a) and (b) Normalized input pulse profiles, (c) OR (without threshold) and AND (with threshold) logic gates at $I_o = 6.5 \times 10^{11}$ W/cm^2, $\beta = -1 \times 10^{-11}$ cm/W, $L = 1$ mm and $\tau_P = 40$ fs (colour online)

A single-input ultrafast AO NOT logic gate at $I_o = 4.8 \times 10^{12}$ W/cm^2 has been theoretically designed as shown in Fig. 7. When a pulse is incident on the sample, a reduction in transmittance occurs because of RSA, resulting in the NOT logic with a percentage modulation of 70%.

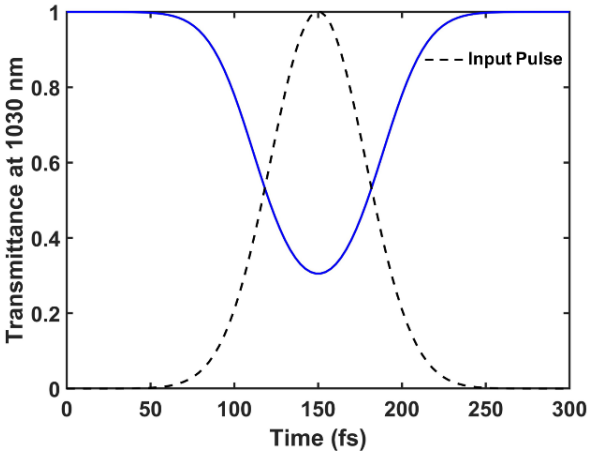

Fig. 7. Time-dependent change in output transmittance at 1030 nm and design of ultrafast AO NOT logic gate at $I_o = 4.8 \times 10^{12}$ W/cm^2, $L = 2$ mm and $\tau_P = 40$ fs (colour online)

The RSA properties at 1030 nm have been utilized to theoretically design ultrafast AO universal NAND and NOR logic gates using two input pulses of equal intensity, each with $I_o = 2.4 \times 10^{12}$ W/cm^2 as shown in Fig. 8. When the pulses arrive simultaneously, the transmittance decreases in comparison to the individual RSA response. The ultrafast AO NOR logic gate is realized by defining a logic 0 below transmittance value 0.56, where the output remains low if either of the two or both of the pulses are incident and switches to high only in the absence of both pulses. The modulation for NOR logic gate is 44%.

Using the identical setup, an ultrafast AO NAND logic gate is designed by defining a threshold value of transmittance at 0.56 (indicated as dashed line in Fig. 8). Here, the output remains low solely when both pulses arrive together whereas it is high under all other situations. The modulation for NAND logic gate is 24%. The truth table for AO universal logic gates is presented in Table 1.

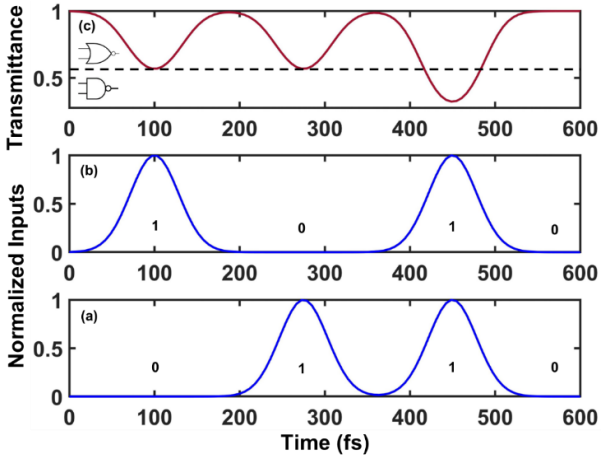

Fig. 8. Time-dependent change in output transmittance at 1030 nm and design of ultrafast AO binary inputs universal logic gates (with a threshold of 0.56, shown by the dashed line): (a) and (b) Normalized input pulse profiles, (c) NOR (without threshold) and NAND (with threshold) logic gates at $I_o = 2.4 \times 10^{12}$ W/cm^2, $L = 2$ mm and $\tau_P = 40$ fs (colour online)

Table 1. Truth table for ultrafast AO binary inputs universal logic gates

Input 1 (TW/cm^2) (Logic States)	Input 2 (TW/cm^2) (Logic States)	Normalized Output Transmittance (Logic States)	
		NOR	NAND
0 (0)	0 (0)	1 (1)	1 (1)
0 (0)	2.4 (1)	0.56 (0)	0.56 (1)
2.4 (1)	0 (0)	0.56 (0)	0.56 (1)
2.4 (1)	2.4 (1)	0.32 (0)	0.32 (0)

The theoretically designed ultrafast AO logic gates are capable of parallel implementation. Fig. 9 presents a schematic representation for this, where two input pulses with intensities I_{in1} and I_{in2} passes through the sample.

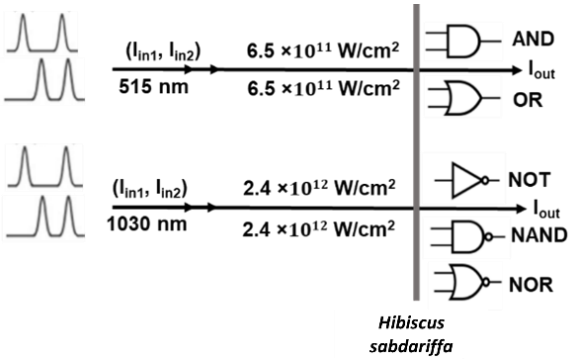

Fig. 9. Diagram illustrating the realization of binary inputs parallel AO logic gates with $I_{in1} = I_{in2}$

For sustained operation, regular pulse excitation is required. Fig. 10 illustrates the effect of pulse frequency at $I_o = 4.8 \times 10^{12}$ W/cm^2. The pulse interval that best maintains the same contrast is 89 fs, with a 70% modulation contrast, resulting in a high bit rate of 11.23 Tb/s. This analysis can help to optimize the bit rate to enable efficient, ultrafast and low-power AO computing.

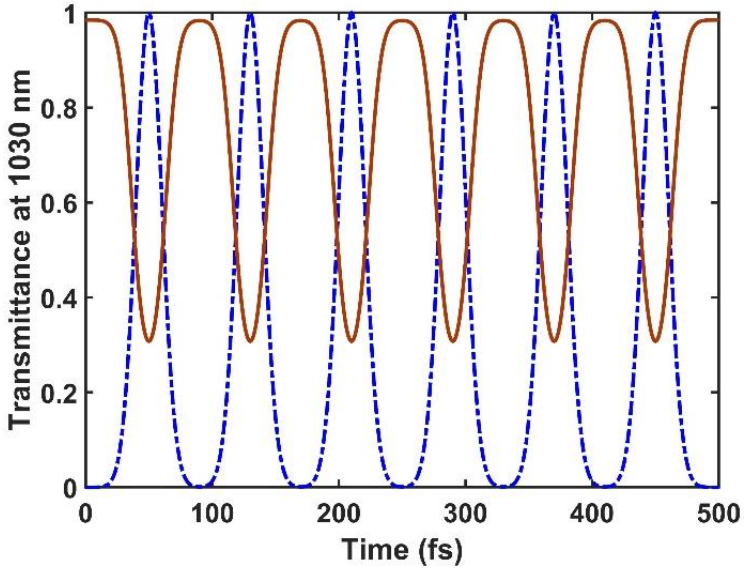

Fig. 10. Effect of pulse frequency at 1030 nm, $I_o = 4.8 \times 10^{12}$ W/cm^2, $\tau_P = 40$ fs, and L = 2 mm (colour online)

An AOD can be theoretically designed using a combination of two nonlinear materials that exhibit SA and RSA [62–64]. Instead of using two separate materials for SA and RSA, a single material that displays both effects based on changes in I_o, λ, L, τ_P, or concentration can be employed to design an AOD. Here, an AOD has been designed by simply adjusting the wavelength rather than combining two distinct materials exhibiting SA and RSA behaviour. In the forward bias, a fs pulse passing through the sample at 515 nm would exhibit an SA response, leading to a sharp increase in light transmission as shown in Fig. 11(a). Reverse bias occurs when the wavelength is switched to 1030 nm, where the sample exhibits RSA, resulting in intensity attenuation as shown in Fig. 11(b). Nonreciprocal transmission of an AOD is achieved theoretically with a nonreciprocity of 3.28 dB, as shown in Fig. 11(c).

The SA and RSA characteristics in *Hibiscus sabdariffa* dye occur at lower intensities compared to those observed in CuPc-doped PMMA nanofilms [14]. The modulation for the AO NAND gate with *Hibiscus sabdariffa* dye and $MoTe_2$ nanofilms is 24% and 8%, respectively [23]. The modulation for AO NOR gate with *Hibiscus sabdariffa* dye and CuPc-doped PMMA thin films is 44%, and 20%, respectively. The NLO characteristics of different organic materials are presented in Table 2, which shows that *Hibiscus sabdariffa* dye has an NLO coefficient comparable to those of the other organic materials. The NLO properties of *Hibiscus sabdariffa* in dye form can differ significantly when the same material is analysed as a thin film due to changes in molecular orientation, concentration, and interactions between the molecules and the substrate [65]. The NLO characteristics of *Hibiscus sabdariffa* dye can be tailored across a broad wavelength spectrum using different approaches, such as modifying its chemical structure or chemically bonding it with materials that display strong NLO responses to create hybrid materials [66]. The synergy between multiple nonlinear processes and the significant interactions resulting from light-driven electron or energy migration within these composite materials enhances the NLO characteristics. As a result, *Hibiscus sabdariffa* dye is a prospective material for photonic applications owing to its NLO characteristics.

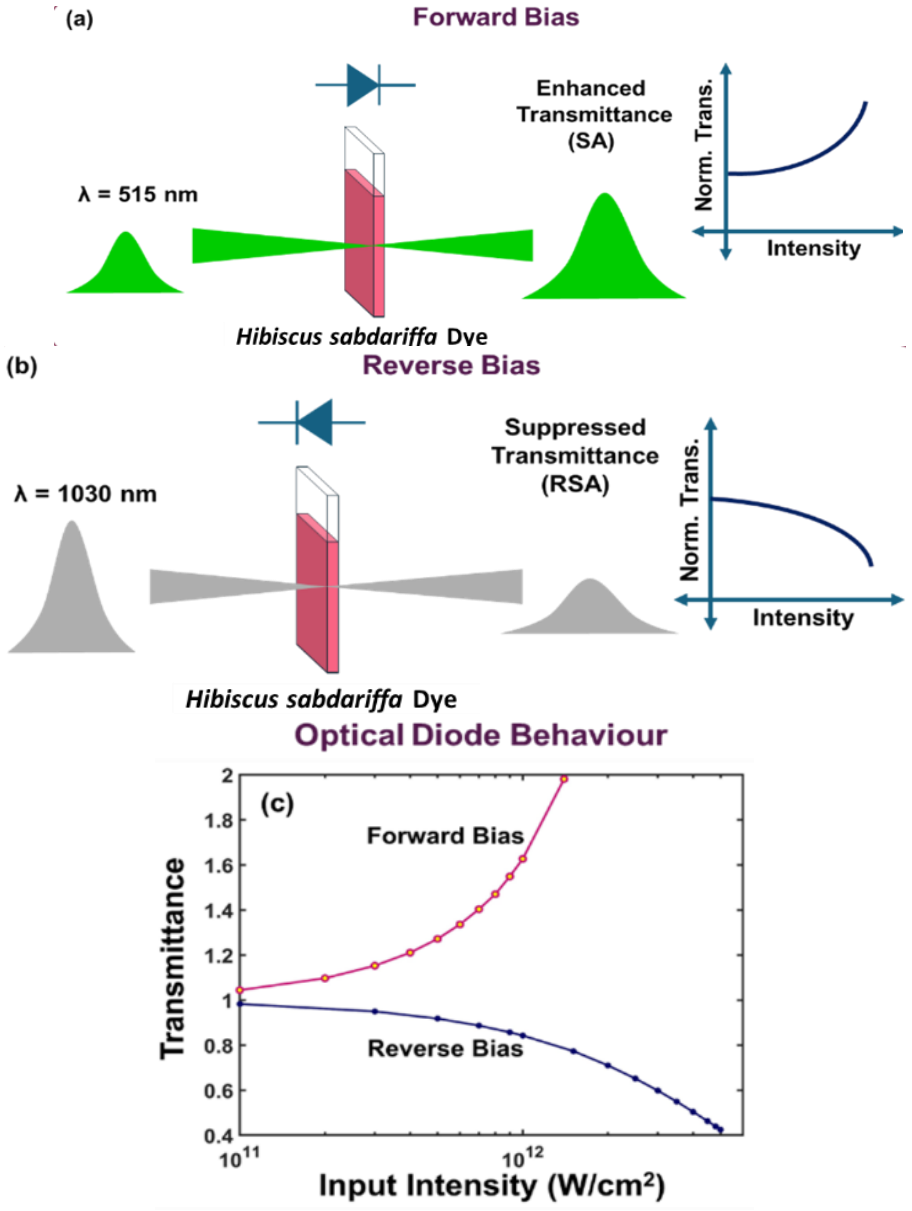

Fig. 11. Illustration of an AOD configuration: (a) Forward, (b) Reverse bias configurations, and (c) Theoretically designed AOD characteristics with Hibiscus sabdariffa dye (colour online)

Table 2. Comparison of NLA coefficient of different organic materials

Materials	λ (nm), τ_P (fs)	I_0 (W/cm^2)	β (cm/W)	Ref.
Hibiscus sabdariffa	1030, 40	(2.8-4.9) ×10^{12}	(2.1 ± 0.4) ×10^{-13}	[50]
	515, 40	7.1×10^{11}-1.4×10^{12}	(-2.7 ± 0.5) ×10^{-11}	[50]
Poly(ε-caprolactone) (PCL) and gold (Au) nanocomposite	800, 90	2.37 × 10^{12}	-6.02×10^{-11}	[67]
Polyether(ether)ketone (PEEK)	387, 180	~3 × 10^{9}	~3.8×10^{-8}	[68]
Fe_2O_3 Hexagonal nanostructures	800, 100	10^{16}-10^{17}	10^{-13}	[69]
Black Phosphorus quantum dots	800, 60	(11.59-28.12) ×10^{9}	(−7.78 ± 0.4) ×10^{-11}	[70]
	1550, 65	1.05×10^{11}-1.30×10^{12}	(4.39 ± 0.15) ×10^{-11}	[70]

4. Conclusion

A comprehensive theoretical study of the ultrafast wavelength-dependent SA and RSA in *Hibiscus sabdariffa* dye has been carried out with fs laser pulses of pulse width 40 fs at 515 nm and 1030 nm, respectively. The formulated theoretical model has been validated by comparing simulated results with recently reported ultrafast z-scan open aperture experimental results, which are in good agreement. The effect of I_o, L and β on SA and RSA characteristics has been studied and further optimized for implementing various ultrafast AO Boolean logic gates namely, NOT, AND, OR, and universal NAND and NOR. The maximum percentage modulation is 97.16% at $I_o = 4.9 \times 10^{12}$ W/cm^2, and L = 2 mm. The RSA characteristics have also been utilized to propose an optical limiter. At $I_o = 2.4 \times 10^{12}$ W/cm^2, the modulation for all-optical NOR and NAND logic gates is 44% and 24%, respectively. The suitability of *Hibiscus sabdariffa* dye for optical limiting has also been studied. The pulse interval that best maintains the same contrast is 89 fs, with a 70% modulation contrast, resulting in a high bit rate of 11.23 Tb/s. A wavelength-dependent AOD has been designed based on axially asymmetric NLA which results in nonreciprocity of 3.28 dB. These results show that the ultrafast NLA characteristics of *Hibiscus sabdariffa* dye can be useful for ultrafast all-optical computing applications.

Acknowledgements

AS and SR express their gratitude to the Department of Science and Technology (DST), India, for providing the INSPIRE Fellowship (DST/ INSPIRE/03/2021/001130) and research grants CRG/2021/005139 and MTR/2021/000742, respectively.

References

[1] V. Rutckaia, J. Schilling, Nature Photonics **14**, 4 (2020).
[2] Z. Chai, X. Hu, F. Wang, X. Niu, J. Xie, Q. Gong, Advanced Optical Materials **5**, 1600665 (2017).
[3] V. Sasikala, K. Chitra, Journal of Optics **47**, 307 (2018).
[4] P. L. McMahon, Nature Reviews Physics **5**, 717 (2023).
[5] F. Höglsperger, B. E. Vos, A. D. Hofemeier, M. D. Seyfried, B. Stövesand, A. Alavizargar, L. Topp, A. Heuer, T. Betz, B. J. Ravoo, Nature Communications **14**, 3760 (2023).
[6] F. Corrado, U. Bruno, M. Prato, A. Carella, V. Criscuolo, A. Massaro, M. Pavone, A. B. Muñoz-García, S. Forti, C. Coletti, O. Bettucci, F. Santoro, Nature Communications **14**, 6760 (2023).
[7] Z.-Z. Ma, Q.-H. Li, Z. Wang, Z.-G. Gu, J. Zhang, Nature Communications **13**, 6347 (2022).
[8] A. Basiri, M. Z. E. Rafique, J. Bai, S. Choi, Y. Yao, Light: Science and Applications **11**, 102 (2022).
[9] S. Roy, C. Yadav, Applied Physics Letters **103**, 241113 (2013).
[10] C. Yadav, S. Roy, Journal of Computational Electronics **14**, 209 (2015).
[11] Y.-W. Kwon, D. Hoon Choi, J.-I. Jin, Polymer Journal **44**, 1191 (2012).
[12] L. Wu, K. Chen, W. Huang, Z. Lin, J. Zhao, X. Jiang, Y. Ge, F. Zhang, Q. Xiao, Z. Guo, Y. J. Xiang, J. Q. Li, Q. L. Bao, H. Zhang, Advanced Optical Materials **6**, 1800400 (2018).
[13] G. Song, X. Wu, W. Zhou, J. Xiao, X. Zhang, Y. Wang, Y. Song, Optical Materials **136**, 113394 (2023).
[14] S. Roy, C. Yadav, Optics Communications **284**, 4435 (2011).
[15] S. Roy, C. Singh, K. Reddy, Applied Physics Letters **77**, 2656 (2000).
[16] C. Singh, S. Roy, Optical Engineering **43**, 426 (2004).
[17] S. Roy, C. Yadav, Laser Physics Letters **11**, 125901 (2014).
[18] S. Roy, P. Sethi, J. Topolancik, F. Vollmer, Advances in Optical Technologies **2012**, 727206 (2012).
[19] S. Krekic, M. Mero, A. Dér, Z. Heiner, The Journal of Physical Chemistry C **127**, 1499 (2023).
[20] A. Szukalski, D. Zajac, N. Pardus, H. E. Karout, P. Krawczyk, B. Sahraoui, Advanced Optical Materials **12**, 2303156 (2024).
[21] C. D. Hutchison, J. M. Baxter, A. Fitzpatrick, G. Dorlhiac, A. Fadini, S. Perrett, K. Maghlaoui, S. B. Lefèvre, V. Cordon-Preciado, J. L. Ferreira, V. U. Chukhutsina, D. Garratt, J. Barnard, G. Galinis, F. Glencross, R. M. Morgan, S. Stockton, B. Taylor, L. Yuan, M. G. Romei, C.-Y. Lin, J. P. Marangos, M. Schmidt, V. Chatrchyan, T. Buckup, D. Morozov, J. Park, S. Park, I. Eom, M. Kim, D. Jang, H. Choi, H. J. Hyun, G. Park, E. Nango, R. Tanaka, S. Owada, K. Tono, D. P. DePonte, S. Carbajo, M. Seaberg, A. Aquila, S. Boutet, A. Barty, S. Iwata, S. G. Boxer, G. Groenhof, J. J. van Thor, Nature Chemistry **15**, 1607 (2023).
[22] Y. Zhang, F. Zhang, B. Du, H. Chen, S. Wageh, O. A. Al-Hartomy, A. G. Al-Sehemi, B. Zhang, H. Zhang, Frontiers of Physics **18**, 33301 (2023).
[23] A. Saifi, S. Roy, Laser Physics Letters **33**, 125402 (2023).
[24] A. Saifi, S. Roy, Journal of Nonlinear Optical Physics and Materials **34**, 2450018 (2025).
[25] A. Saifi, S. Roy, Journal of Nonlinear Optical Physics and Materials **34**, 2450029 (2025).
[26] C. Yadav, S. Roy, Optical and Quantum Electronics **48**, 1 (2016).
[27] C. Yadav, S. Roy, Optical and Quantum Electronics **49**, 25 (2017).
[28] H. Bansal, N. Gupta, S. Roy, Journal of Neural Engineering **18**, 0460b8 (2021).
[29] N. Gupta, H. Bansal, S. Roy, Neurophotonics **6**, 025002 (2019).
[30] S. Saran, N. Gupta, S. Roy, Neurophotonics **5**, 025009 (2018).

[31] A. Dharmadhikari, B. Roy, S. Roy, J. Dharmadhikari, A. Mishra, G. R. Kumar, Optics Communications **235**, 195 (2004).
[32] F. A. Samad, M. S. Abdel-wahab, W. Z. Tawfik, H. Qayyum, R. Apsari, T. Mohamed, Optical and Quantum Electronics **55**, 753 (2023).
[33] M. Ashour, M. S. Abdel-Wahab, A. Shehata, W. Z. Tawfik, M. Azooz, S. A. Elfeky, T. Mohamed, Journal of the Optical Society of America B **39**, 508 (2022).
[34] S. Mohamed, F. Abdel Samad, M. Ashour, M. S. Abdel-Wahab, W. Z. Tawfik, V. R. Soma, T. Mohamed, Applied Optics **61**, 7283 (2022).
[35] A. N. Hassan, M. A. Haddad, A. Behjat, M. Golestanifar, Scientific Reports **14**, 18158 (2024).
[36] N. Numan, S. Jeyaram, K. Kaviyarasu, P. Neethling, J. Sackey, C. Kotsedi, M. Akbari, R. Morad, P. Mthunzi-Kufa, B. Sahraoui, M. Maaza, Scientific Reports **12**, 9078 (2022).
[37] S. R. Marder, W. E. Torruellas, M. Blanchard-Desce, V. Ricci, G. I. Stegeman, S. Gilmour, J.-L. Bredas, J. Li, G. U. Bublitz, S. G. Boxer, Science **276**, 1233 (1997).
[38] A. G. Faisal, Q. M. Hassan, T. A. Alsalim, H. Sultan, F. S. Kamounah, C. Emshary, Journal of Physical Organic Chemistry **35**, e4401 (2022).
[39] F. Z. Henari, K. E. Jasim, Applied Physics B **112**, 261 (2013).
[40] S. Jeyaram, T. Geethakrishnan, Optical Materials **107**, 110148 (2020).
[41] S. Jeyaram, Brazilian Journal of Physics **52**, 24 (2022).
[42] S. Jeyaram, D. J. Rany, Journal of Fluorescence **33**, 287 (2023).
[43] B. Anusha, S. Devanesan, M. S. AlSalhi, G. Murali, M. Vimalan, S. Madhu, S. Jeyaram, Journal of Optics **54**, 979 (2025).
[44] S. Jeyaram, A. G. B. Dileepan, M. Vishalatchi, K. Jayasheela, S. Murali, M. A. Wadaan, N. D. Almoutiri, S. O. Oseni, M. Santhamoorthy, Scientific Reports **16**, 2769 (2026).
[45] S. Biswas, P. Kumbhakar, Spectrochimica Acta Part A: Molecular and Biomolecular Spectroscopy **173**, 400 (2017).
[46] M. Rahma, H. Saadon, AIP Conference Proceedings **2190**, 1 (2019).
[47] A. Thankappan, S. Thomas, V. Nampoori, Optical Materials **35**, 2332 (2013).
[48] D. Ramírez-Martínez, E. Alvarado-Méndez, M. Trejo-Durán, M. Vázquez-Guevara, Optics Express **22**, 25161 (2014).
[49] S. Afanador-Delgado, R. Sevilla-Escoboza, V. Marañón-Ruíz, R. Chiu, Optics and Laser Technology **132**, 106468 (2020).
[50] A. A. Baker, G. S. Boltaev, P. Piatkowski, M. Khamis, A. S. Alnaser, Optical Materials **138**, 113728 (2023).
[51] A. Diallo, S. Zongo, P. Mthunzi, S. Rehman, S. Alqaradawi, W. Soboyejo, M. Maaza, Applied Physics B **117**, 861 (2014).
[52] E. Hoque, M. Biswas, A. Somadder, M. Faruk, S. Sharif, N. Chawdhury, S. Das, Y. Haque, Journal of Optics **42**, 286 (2013).
[53] F. Henari, A. Al-Saie, Laser Physics Letters **16**, 1664 (2006).
[54] M. A. Salawu, A. A. Ayobami, A. Adebisi, S. C. Ezike, Y. O. Saheed, A. B. Alabi, Optical Materials **127**, 112177 (2022).
[55] L. Komalavalli, P. Amutha, S. Monisha, Materials Today: Proceedings **33**, 2279 (2020).
[56] S. Mohandoss, N. Ahmad, K. S. Velu, M. R. Khan, S. Palanisamy, S. You, Y. R. Lee, Chemosensors **11**, 474 (2023).
[57] F. Li, X. Li, Optics Communications **285**, 5217 (2012).
[58] J. Oberle, L. Bramerie, G. Jonusauskas, C. Rulliere, Optics Communications **169**, 325 (1999).
[59] C. Li, K. Yang, Y. Feng, X. Su, J. Yang, X. Jin, M. Shui, Y. Wang, X. Zhang, Y. Song, H. Y. Xu, The Journal of Physical Chemistry B **113**, 15730 (2009).
[60] J. Li, L. Du, J. Huang, Y. He, J. Yi, L. Miao, C. Zhao, S. Wen, Nanophotonics **10**, 927 (2020).
[61] R. L. Sutherland, Handbook of Nonlinear Optics, CRC Press, 2003.
[62] J. Mu, Z. Yang, Q. Zhang, X. Yuan, G. Wang, H. Qi, F. Wang, W. Sun, Journal of Materials Science **58**, 11527 (2023).
[63] R.-N. Verrone, C. Moisset, F. Lemarchand, A. Campos, M. Cabié, C. Perrin-Pellegrino, J. Lumeau, J.-Y. Natoli, K. Iliopoulos, ACS Applied Nano Materials **3**, 7963 (2020).
[64] K. Wang, M. Seidel, K. Nagarajan, T. Chervy, C. Genet, T. Ebbesen, Nature Communications **12**, 1486 (2021).
[65] S. Mathews, S. C. Kumar, L. Giribabu, S. V. Rao, Materials Letters **61**, 4426 (2007).
[66] S. Saha, B. T. Diroll, M. G. Ozlu, S. N. Chowdhury, S. Peana, Z. Kudyshev, R. D. Schaller, Z. Jacob, V. M. Shalaev, A. V. Kildishev, A. Boltasseva, Nature Communications **14**, 5877 (2023).
[67] F. B. Sariipek, Y. Gündoğdu, H. Ş. Kiliç, Optical Materials **129**, 112556 (2022).
[68] Q. Li, W. Perrie, Y. Tang, O. Allegre, J. Ho, P. Chalker, Z. Li, S. Edwardson, G. Dearden, Procedia CIRP **94**, 840 (2020).
[69] P. Thomas, P. Sreekanth, K. Abraham, Journal of Applied Physics **117**, 053103 (2015).
[70] R. Chen, X. Zheng, T. Jiang, Optics Express **25**, 7507 (2017).

*Corresponding author: sukhdevroy@dei.ac.in